[Frontiers in Bioscience E3, 395-409, January 1, 2011]

The respiratory-dependent assembly of ANT1 regulates cytochrome *c* release

Faustin Benjamin [1], Rossignol Rodrigue [1], Deniaud Aurelien [2], Rocher Christophe [1], Claverol Stephane [3], Malgat Monique[1], Brenner Catherine [4], Letellier Thierry [1]

[1]INSERM U688, Universite Victor Segalen-Bordeaux 2, 146 rue Leo-Saignat, F-33076 Bordeaux Cedex, France, [2]University of Versailles/St Quentin, PRES UniverSud Paris, CNRS UMR 8159, Bat Buffon, 45 avenue des Etats-Unis, F-78035 Versailles, France, [3]Centre de genomique fonctionnelle, Universite Victor Segalen-Bordeaux 2, 146 rue Leo-Saignat, F-33076 Bordeaux Cedex, France, [4] Univ Paris-Sud, INSERM UMR-S 769, PRES UniverSud Paris, Châtenay-Malabry, 92290, France

TABLE OF CONTENTS

1. ABSTRACT

The adenine nucleotide translocator (ANT) is a control point of several fundamental cell processes, as diverse as cell energy supply, mitochondrial DNA maintenance, and apoptosis. This paper describes six individual structures of the carrier, distinguished according to ANT1 oligomeric and conformational states, as well as associations with other proteins. Transitions between these structures depend on energy demand and thus contribute to a metabolic reserve of oxidative phosphorylation (OXPHOS) activity. Moreover, at low respiratory chain activity, we demonstrate that, unlike a mitochondrial Ca^{2+} upload, Bax, a pro-apoptotic Bcl-2-family protein, is able to trigger a massive release of cytochrome *c* from one of these ANT1 structures. These new insights emphasize the close relationship between structural rearrangements of ANT and molecular apoptotic events at distinct cell energy levels. OXPHOS functioning has to therefore be considered a crucial control point for the events leading to these contrasting pathways.

2. INTRODUCTION

The adenine nucleotide translocator (ANT) plays an essential role in the oxidative phosphorylation (OXPHOS) system developed in aerobic eukaryotic cells. One of the major functions of this nuclear encoded protein is to catalyze the exchange between cytosolic ADP and ATP synthesized within mitochondria. This exchange consequently provides the energy for several ATP-dependent functions occurring within the cell (1). The carrier can be specifically inhibited and stabilized into two distinct conformations, i.e. cytosolic *c* or matricial *m*, induced by binding carboxyatractyloside (CATR) or bongkrekic acid (BA), respectively (2).

Various ANT isoforms are expressed in mammalian cells, i.e. ANT1 is known as the specific heart/muscle isoform but is also expressed to a lesser extent in kidney and brain (3). It is now assumed that the minimal functional state of this carrier is the homo-dimer (4). However, several oligomerization states, such as tetramers

or coupled dimers, have emerged from nucleotide binding data (5). In addition to this role in bioenergetics, ANT remains crucially involved in mtDNA maintenance (6). Besides these living functions, this carrier also plays a key role in programmed cell death (7; 8). ANT1 is described as a core component in the permeability transition pore complex (PTPC), as its large opening under diverse apoptotic stimuli, such as Ca^{2+} upload, leads to mitochondrial membrane potential ($\Delta\Psi_m$) collapse (9). PTPC is essential promoting the pro-apoptotic effect of Bax by forming pores in the external membrane and, thus, making it possible for apoptogenic factors, e.g. cytochrome *c* (cyt *c*), to diffuse from mitochondria to the cytosol (10; 11). Another release mechanism, demonstrated in cultured cells, is also mediated by Bax, but independently of PTPC (12; 13).

We recently reported that ANT might adopt various oligomeric and conformational states, changing according to the cell energy state (14). In this research, we demonstrated by analyzing various ANT1 structures using blue-native polyacrylamide gel electrophoresis (BN-PAGE)/ sodium dodecyl sulfate-PAGE (SDS-PAGE) that there could be up to six different forms of ANT1 in functional muscle mitochondria. We showed that these structures contribute to a metabolic reserve of oxidative phosphorylation (OXPHOS) activity through ANT1 oligomerization and conformational changes from a PTPC-like structure. These mechanisms enable OXPHOS to adapt to mitochondrial mutations or various cell energy states. Moreover, we suggest that one of the complexes formed by the interaction of ANT1 monomer with VDAC1 and endogenous Bax monomer forms a control point in the dual mitochondrial functions of energy production and apoptosis. Indeed, this structure is associated with 80% of the mitochondrial cyt *c* content at low OXPHOS activity. However, at higher energy states, ANT1 oligomerization leads to disassociate cyt *c* from this complex, thus responding to a respiratory flux increase.

In addition, we show that the recombinant proapoptotic protein Bax is able to target this structure, inducing a massive release from the bound pool of cyt c. This suggests this complex may be implicated in apoptosis, thus constituting an "apoptotic induction unit" for cyt *c* release, independent of the SMAC/Diablo release pathway. In contrast, the Ca^{2+}-induced permeability transition triggers the release of free-respiratory active cyt *c*, thereby affecting mitochondrial energy functions.

As we have shown, ANT is a control point in the cell metabolism, enabling the respiratory chain to adapt to varying energy demands, as well as having a regulatory function in programmed cell death.

3. MATERIAL AND METHODS

3.1. Animals and mitochondrial preparations

All the methods are fully described in (15). Protein concentration was estimated by the Biuret method.

3.2. Human muscle biopsies

Three patients were selected at the Centre Hospitalier Regional de Bordeaux and diagnosed by clinical investigations, biological studies (especially blood lactate and pyruvate), and histo-enzymological studies. Controls were taken from patients who underwent muscle biopsy for neuromuscular symptoms, but were ultimately found to be free of any mitochondrial disease. Muscle biopsies were performed on the quadriceps muscle under general anesthesia (with the informed consent of the patients or their parents). Muscle biopsies were stored in 10 ml ice-cold buffer (EGTA 10 mM, $MgCl_2$ 5 mM, taurine 20 mM, dithiothreitol 0.5 mM, imidazol 20 mM, K^+MES 0.1 M, ATP 5 mM, phosphocreatine 20 mM) and used in the following hour. The mitochondrial respiratory rate was measured on saponin- permeabilized muscle fibers, using the procedures developed by (16). Mitochondrial oxygen consumption on various respiratory substrates was measured as described in a medium containing 10 mM EGTA, 5 mM $MgCl_2$, 20 mM taurine, 0.5 mM dithiothreitol, 20 mM imidazol, 0.1 M K^+MES, 3 mM KH_2PO_4, 5mg/ml BSA, and expressed in natomO/min/mg of fibers.

3.3. Oxygraphic and swelling measurements

Mitochondrial oxygen consumption was monitored at 30°C in a 1 ml thermostatically-controlled chamber equipped with a Clark oxygen electrode connected to a computer, which gave an on-line display of the respiratory rate value. The respiration buffers were used as described in (15), with the addition of respiratory substrates (10 mM pyruvate with 10 mM malate, or 25 mM succinate with 0.4 µg/ml rotenone, or 3 mM ascorbate with 0.5 mM TMPD, or 2 µM CCCP. However, in the case of Ca^{2+} addition, EGTA in the respiration buffer was replaced by 5 µM and the respiratory rate recorded at state 4. The mitochondrial concentration used was 1 mg/ml and state 3 according to (17) was obtained by adding 2 mM ADP. Mitochondrial oxygen consumption was expressed in natomO/min/mg proteins. MPT was measured by the convenient swelling assay, carried out in an Uvikon 940 spectrophotometer. Swelling curves were recorded at 540 nm. Cuvettes containing the mitochondrial suspension were maintained at 25°C. Incubation conditions and MPT induction are indicated in the Figure legends.

3.4. Titration curves, threshold curves, and threshold value determination

Titration curves of the step catalyzed by ANT were performed using CATR (Sigma), as described by (14). Threshold curves come from the titration curves and represent the state 3 respiratory rate (%) as a function of ANT inhibition (%) The threshold values were determined as described (15).

3.5. Production and purification of recombinant BaxΔC

Bax Δ21 was produced as a GST-fusion recombinant protein in *E. coli*. The GST N-terminal tag was cleaved by thrombin and Bax Δ21 was purified as described by (18). To induce oligomerization, Bax Δ21 was incubated with TX-100 (TX-100/protein ratio of 1.4 g/g) at 4°C for 30 min. Mitochondria respiring with different respiratory substrates were then incubated with oligomerized Bax Δ21 at 30°C for 30 min.

3.6. Electrophoresis techniques

Isolated rat mitochondria from muscle (1mg/ml) were subjected to oxygraphic measurements at state 3 on various respiratory substrates. Mitochondrial proteins (300 µg) were taken from the oxygraph, solubilized by digitonin, and then subjected to BN-PAGE/SDS-PAGE procedures, as described (14). However, for the BaxΔC experiments, the ultracentrifugation previously used to remove solubilized complexes was reduced to 20 000 rpm, at 4°C, for 30 min.

3.7. Western-blot

Mitochondrial membrane proteins solubilized by digitonin (digitonin/protein ratio of 3g/g) were subjected to BN-PAGE/SDS-PAGE, electrotransferred to PVDF membranes (Bio-Rad), and subjected to primary ab in 5% milk. Polyclonal abs specific for human ANT1 isoform (Ab1, amino acids 2-11 and Ab2, amino acids 161-171) were purchased from Oncogene Research Products. Abs for Porin (31HL) and cyclophilin D were purchased from Calbiochem; and cytochrome c from Zymed. All abs were used at dilutions recommended by the manufacturer. After washing steps, membranes were incubated with horseradish peroxydase-conjugated purified secondary abs (Bio-Rad) Proteins were detected by enhanced chemiluminiscence (ECL; Amersham Pharmacia) and revealed by autoradiography. For cytochrome *c* release measurements, isolated muscle mitochondria (1mg/ml) respiring with the various substrates at state 4 in the presence of Ca^{2+} were centrifuged (20 min, 8000 rpm, 4°C) The supernatant was then removed with 1µg/ml protease inhibitors (PMSF, leupeptin and pepstatin), subjected to SDS-PAGE (20% SDS, 1% β-mercaptoehanol), and immunoblotted, as described above.

3.8. Protein detection and analysis

The proteins separated by second (m) SDS-PAGE dimension were subjected either to Western-blotting or Sypro Ruby® staining (Molecular Probes), according to the manufacturer's instructions. Fluorescent proteins were detected with an UV-transilluminator system and recorded using a Herada 429K DV camera. The protein spots were cut and subjected to tandem mass spectrometry analysis. Densitometry analysis on Western-blots was carried out using Image J (NIH) software.

4. RESULTS

4.1. Distribution of ANT1 oligomeric and conformational states in functional mitochondria

In a recent study, we showed that ANT1 might exist in several oligomeric states within the inner membrane of muscle mitochondria respiring with ADP on pyruvate-malate (14). Indeed, when membrane proteins were solubilized with digitonin and BN-PAGE/SDS-PAGE coupled with Western-blots using a polyclonal antibody specific for ANT1 (abs, Ab1), we observed the presence of ANT1 monomers, dimer and coupled-dimer functional forms in the ADP/ATP exchange (M_1, D_1, $2D_1$; Figure 1. A) When Ab2 that recognizes the second matricial loop of ANT1, was used, two novel forms were observed, i.e. D_2 dimers (50 kDa) associated with porin in a complex exceeding 300 kDa and free M_2 monomers (31 kDa) (Figure 1A) Thus, when the N-terminal domain (N-ter) was exposed, the second matricial loop was not recognized, and *vice versa*. These results indicate that the two ANT1 conformations, i.e. cytosolic *c* and matricial *m*, are revealed by the two distinct antibodies used.

The proteins potentially bound to ANT1 monomers in the *c* conformation (M_1) within the 75 kDa complex were studied. Sypro ruby® staining of mitochondria respiring on pyruvate-malate with ADP revealed the proteomic pattern (Figure 1Ba) The Western-blot immunoblotted with anti-ANT1 (Ab1), anti-porin, anti CyD and anti-cyt *c* (Figure 1Bb) showed the three ANT1 *c* forms associated with porin, therefore D_1 was also interacting with CyD within the 300 kDa complex. Surprisingly, the 75 kDa complex was composed of M_1, monomeric porin and cyt *c*. In addition, cyt *c* was also observed in a 16 kDa minority free form in the first dimension. Spots indicated in Figure 1Bd was subjected to a tandem mass spectrometry analysis. Peptide sequences compared with the NCBI databank suggest a good correlation for the presence of the ANT isoform 1 in M_1 and M_2 and the voltage-dependent anion-channel isoform 1 (VDAC1) in the 75 kDa complex, and VDAC2 in free state (Xcorr and gi indicated) Unfortunately, the thin fluorescent staining of cyt *c* could not be analyzed by mass spectrometry. Another 100 kDa spot in a complex of over 300 kDa in the first dimension was an association of ANT (isoform not specified) with mitochondrial creatine kinase (mtCK). Figure 1. Bc shows the presence of D_2 (matricial conformation), porin, and CyD within a complex exceeding 300 kDa, as well as free 31 kDa M_2 monomers. As previously shown, Cyt c was co-localized with porin in the 75 kDa complex but a minority was also found in free form.

BN-PAGE on gradient gel was used to characterize the over-300 kDa complexes, under the same conditions as above (Figure 1Be) and OXPHOS complexes were revealed by Blue Coomassie staining. Subunits of each complex were then separated in modified second dimension, stained with Sypro Ruby®, and subsequently immunoblotted with either anti-ANT1 (Ab1) (Figure 1. Bf) or anti-ANT1 (Ab2) (Figure 1Bg), together with anti-porin and anti-CyD. Western-blots showed D_1, porin and CyD associated in a 550-600 kDa complex, on the one hand, and D_2 with porin but not CyD in a 400 kDa complex, on the other hand. The D_2 form of ANT1 also interacted with the two respiratory chain supercomplexes of 1400 and 1600 kDa described by (19). The membrane used with anti-ANT1 (Ab2) was then reprobed with anti-Cyt *c* (Figure 1Bh) and showed that cyt *c* was associated in complexes under 100 kDa in the first dimension.

4.2. Oligomeric and conformational states of ANT1 depend on respiratory chain activity

As previously described (14), the increase in respiration from pyruvate-malate to ascorbate-TMPD via succinate led to a rise in $2D_1$ (contrarily to D_1), accompanied by a considerable decrease in ANT1 M_1

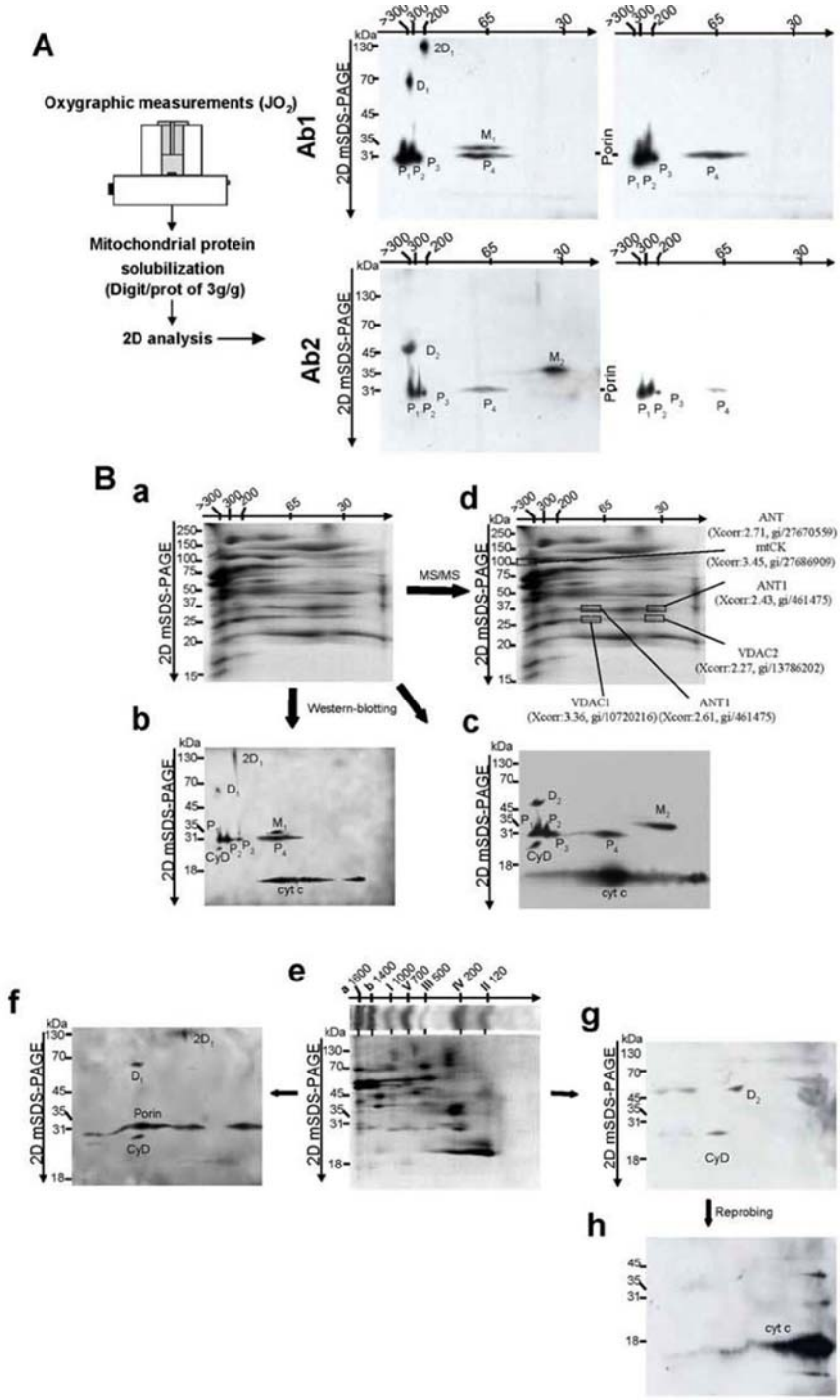

Figure 1. Different oligomers and conformations of ANT1 in functional mitochondria. Cytochrome c is stored by ANT1 monomers stabilized only in the c conformation. (A) 2D gel analysis of muscle mitochondria respiring on pyruvate-malate with ADP, solubilized by digitonin, and subjected to BN-PAGE 10% acrylamide slab gel. The second dimension (SDS/PAGE) was then immunoblotted, using either anti-ANT1 (Ab1) or (Ab2), together with anti-Porin. Gels to the right indicate Porin signals. (Ba) Same procedure but stained with Sypro ruby®; (b) then immunoblotted with anti-ANT1 (Ab1), anti-porin, anti-CyD and anti-cyt c; (c) or with anti-ANT1 (Ab2); (d) the spots indicated were subjected to a tandem mass spectrometry, Xcorr and gi are indicated; or (e) proteins were subjected to 5-13% BN-PAGE gradients and stained with Coomassie blue. OXPHOS complexes (I, II, III_2, IV, V) and "supercomplexes" (a, b) mentioned by (19) are indicated. The second dimension was stained with Sypro-ruby® and (f) subsequently immunoblotted with anti-ANT1 (Ab1), anti-porin and anti-CyD, or with anti-ANT1 (Ab2) and anti-CyD (g) (h) The membrane was then reprobed with anti-cyt c. M_1 and M_2, ANT1 monomers recognized by Ab1 or Ab2; D_1 and D_2, ANT1 dimers; $2D_1$, ANT1 coupled dimers. CyD, cyclophilin D; cyt c, cytochrome c.

Table 1. Respiratory and inhibition parameters obtained in human muscle fibers

Respiratory substrates	JO_2	RCR	K_i	T	I_{max}
Pyruvate-malate -Creatine	2.2±0.4	2.5±0,3	28.4±4.1	85±2.2	0.54±0.11
+Creatine 10 mM	2.9±0.3	3.4±0.6	30.7±2.2	84±1.9	0.91±0.09
+Ca^{2+} 50 μM	3.3±0.4	1.6±0.2	31.1±5.3	N.D.	0.29±0.12
Succinate	4.2±0.7	2.2±0.6	26.5±3.7	88±2.4	0.98±0.08

JO_2: State 3 respiratory rate, in natomO/min/mg of muscle fibers; RCR: respiratory control ratio; K_i (nM): CATR inhibition constant; T (%): threshold values expressed as a percentage of ANT inhibition; I_{max} (nmol/mg): amount of CATR necessary to return from state 3 to state 4 respiration. Results are presented in the curves as mean ± S.E. from three different patients investigated.

monomers, which were no longer observed on ascorbate-TMPD (Figure 2A) Interestingly, adding CCCP uncoupler disassociated the ANT1 oligomers and ANT1-porin associations, resulting in an increase in M_1. As for Ab1, M_2 forms were expressed more than D_2, but no coupled dimers in the *m* conformation were detected (Figure 2A) By replacing pyruvate-malate with succinate, the increase in D_2 content was followed by synthesis of coupled dimers in the *m* conformation ($2D_2$, 110 kDa) Unlike $2D_1$, all $2D_2$ forms were associated with complexes over 300 kDa. When respiration was further increased on ascorbate-TMPD, $2D_2$ forms increased considerably compared to D_2 whereas M_2 was no longer observed. Adding CCCP induced the same disassociation effect on the *m* structures. Consequently, these two types of ANT1 monomers are able to constitute preferentially coupled dimeric structures, irrespective of their *c* or *m* conformation. However, each oligomer conformation interacts with specific macrocomplexes.

In order to analyze these respiratory-induced transitions for complexes exceeding 300 kDa, we carried out the same procedure using 5-13% gradient BN-PAGE. The second modified dimension was immunoblotted with either anti-ANT1 (Ab1) or anti-ANT1 (Ab2) and reprobed with anti-CyD and anti-porin (Figure 2B) Porin signals were used to quantify the various ANT1 forms. As in Figure 1. Bf and Bg, D_1 was associated with porin and CyD with a 550-600 kDa complex, unlike D_2, which was associated with porin but not CyD in a 400 kDa complex. Small amounts of the latter structure were also associated with two respiratory chain supercomplexes. As previously shown, the respiratory increase from pyruvate-malate to ascorbate-TMPD induced an increase in both $2D_1$ and $2D_2$ content. However, while $2D_1$ interacted with porin in a 220 kDa complex, $2D_2$ was mainly associated with the 1600 kDa supercomplex on ascorbate-TMPD. Nevertheless, the transition from pyruvate-malate to succinate led to a larger decrease in D_1 than CyD (2 fold and 1.4 fold, respectively), while D_2 increased in both cases. These observations may indicate that an additional structural mechanism occurs at lower fluxes besides oligomerization.

4.3. ANT may be mobilized from a structure responsible for the mitochondrial permeability transition

In Figure 2B, the amount of D_1 followed the decrease in M_1 when respiration is raised from pyruvate to succinate, unlike D_2, which increased under the same respiratory conditions. This suggests that there are two distinct mechanisms, depending on the respiratory chain activity level, i.e. (i) a mobilization of monomers as described above and (ii) probably conformational changes in the carrier for lower transitions of respiratory steady-states. On permeabilized human muscle fibers, we titrated the mitochondrial respiration by CATR and determined the amount of functional ANT involved in the flux (Figure 3 A) The amount of inhibitor necessary to inhibit all the carriers involved in the flux (Imax), as well as the inhibition constant (Ki) are given in Table 1. As previously observed, the amount of ANT participating in the respiratory steady-state increased when pyruvate-malate was replaced with succinate (less than 2-fold), but the Ki values remained constant. Likewise, adding 10 mM creatine in the presence of pyruvate-malate with ADP increased both the respiratory steady-state and the Imax value, almost to the same extent as succinate (Table 1) Moreover, the Ki value also remained constant. On the contrary, adding Ca^{2+} in the presence of pyruvate-malate with ADP induced an uncoupling of respiration and decreased the Imax value by half. Threshold curves shown in Figure 3, B represent the effect of ANT inhibition by CATR on the respiratory rate. Our results show that ANT activity can be inhibited by up to 80% on pyruvate-malate with or without creatine, with only a slight effect on respiration. However, this excess enzyme activity was not observed with Ca^{2+}, as there was only half the functional ANT in the ADP/ATP exchange. Creatine was recently found to inhibit the permeability transition by enhancing the microcompartmentation between ANT and mtCK (20). Moreover, we show here that its addition in the cell context makes it possible to increase the functional amount of ANT. This effect probably occurs through conformational changes in the carriers from the *c* state within a PTP-like structure with CyD to the *m* state associated with mtCK.

4.4. Cytochrome c is mobilized through the respiratory-induced oligomerization of ANT1

As described in Figure 1, cyt *c* is mainly associated with porin and M_1 in the 75 kDa complex. Furthermore, small amounts have also observed in free-state in mitochondria respiring on pyruvate-malate with ADP. Likewise, Figure 4. A shows that, under these conditions, 81% of cyt *c* is associated. When respiration increased from pyruvate-malate to succinate, the decrease in bound cyt *c* was concomitant with a proportional increase in the free-state (Bar graphs in Figure 4A) This phenomenon is more marked between succinate and ascorbate-TMPD as the bound state completely disappears in favor of the free form (80% of total cyt *c* increase). We reproduced the same experiments in brain and liver mitochondria, known to express ANT1 (to a lesser extent than muscle) and, mainly, ANT2 (Figure 4B) We observed the presence of bound cyt *c* in brain (less than in muscle) but not in liver. Thus, this cyt *c* mobilization,

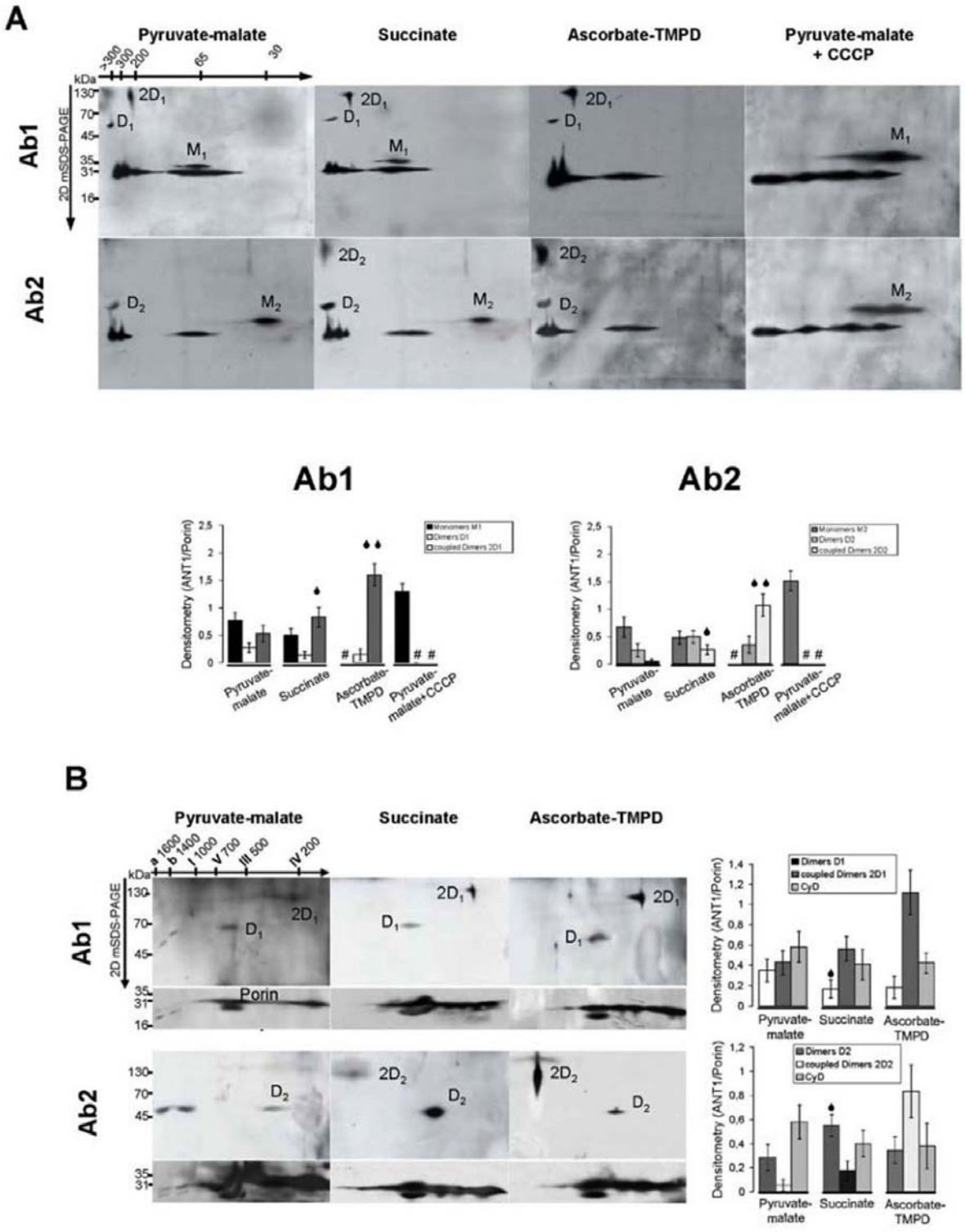

Figure 2. Oligomeric and conformational distributions of ANT1 vary upon distinct respiratory chain activities. (A) 2D gel analysis with 10% BN-PAGE or (B) 5-13% gradients of muscle mitochondria solubilized with digitonin and respiring with ADP on the various substrates indicated. Second dimensions were immunoblotted with either Ab1 or Ab2, together with anti-Porin and anti-CyD (for gradients) ANT1 monomers M_1 and M_2, dimers D_1 and D_2, and coupled dimers $2D_1$ and $2D_2$ were quantified by densitometry and normalized by Porin signals. Densitometry analyses are presented in bar graphs as mean ± S.E. (n=3) *, $P<0.05$ versus $2D_1$ or $2D_2$ (or D_1 or D_2) on pyruvate-malate; **, $P<0.05$ versus $2D_1$ or $2D_2$ on succinate; #, ANT1 forms not detected.

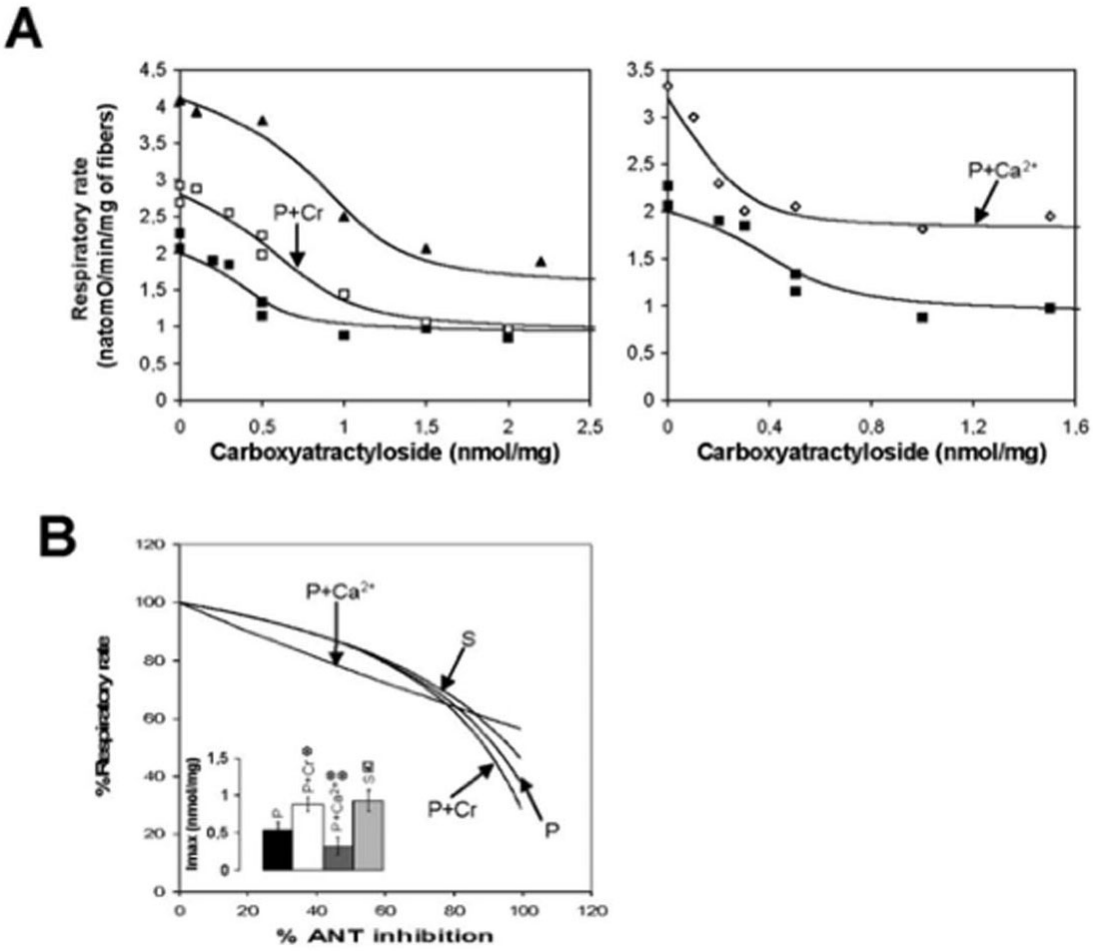

Figure 3. ANT mobilization occurs in human muscle fibers following changes in respiratory substrates. Example of titration and threshold curves obtained from a single muscle biopsy. (A) Human fibers taken from biopsies were permeabilized by saponin and state 3 respiratory rate with ADP was inhibited by CATR on pyruvate-malate with (□) or without (■) creatine 10 mM, or succinate (▲) Same procedure is realized on pyruvate with (O) or without (■) Ca^{2+} 50 µM. (B) Threshold curves on pyruvate-malate (P), succinate (S), pyruvate-malate with creatine (P+Cr), and pyruvate-malate with Ca^{2+} (P+Ca^{2+}) Respective Imax obtained from three patients are indicated in the bar graphs. *, P<0.05 versus pyruvate-malate; **, P<0.05 versus pyruvate-malate; ❖, P<0.05 versus pyruvate-malate.

mainly in response to high fluxes, depends on the amount of ANT1 and is linked to M_1 oligomerization.

Cyt *c* in the 75 kDa complex may be more tightly bound to the inner membrane than in its free state. In Figure 5, we added various concentrations of Ca^{2+} and analyzed the cyt *c* release capacities at the different respiratory chain activity levels induced. In isolated mitochondria, a low matricial Ca^{2+} uptake was sufficient to induce a permeability transition leading to the release of several apoptogenic factors, such as cyt *c* (21). Figure 5A shows that cyt *c* was mainly released by Ca^{2+} as the respiratory rate increased. This effect was inhibited by 10 µM CsA, whereas adding CCCP induced a strong release compared to pyruvate-malate only. As control, we showed that the mitochondrial swelling induced by adding 100 µM Ca^{2+} was strictly the same, irrespective of the energy substrate used (Figure 5A)

To determine whether the cyt *c* pool was affected by Ca^{2+}, we analyzed 2D gels of mitochondria respiring on various substrates in the presence of 100 µM Ca^{2+} (Figure 5B) As shown in the densitometry analysis, this addition induced a decrease in bound cyt *c* (C_b) and an increase in free cyt *c* (C_f) This mobilization of cyt *c* resulted from the uncoupling effect of Ca^{2+} responsible for increasing respiration. However, this effect was attenuated as respiration continued to increase. Consequently, the released cyt *c* seems to follow ANT mobilization when respiration increases. This indicates that interactions within the 75 kDa complex may confer a tight binding of cyt *c* stored within the inner membrane, as compared to the

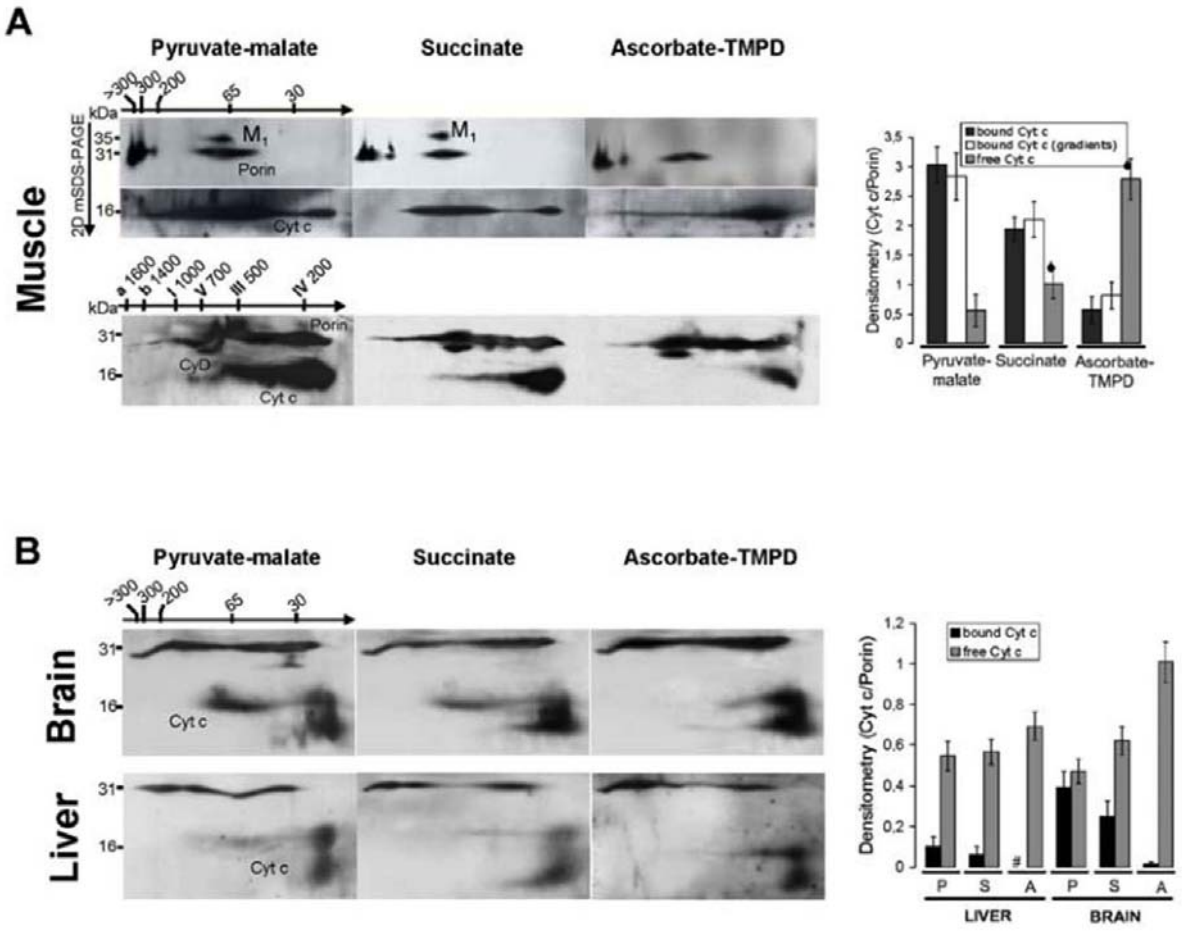

Figure 4. Tightly bound cytochrome c is mobilized as free form and becomes involved in electron transfer through the respiratory chain. (A) 2D gel analysis with either 10% (gels to the top) or 5-13% gradient BN-PAGE of muscle mitochondria solubilized with digitonin and respiring with ADP on the various substrates. Second dimensions were immunoblotted with Ab1 and anti-Porin, and reprobed with anti-cyt c. Gradient gels were immunoblotted with anti-porin, anti-CyD, and anti-cyt c. Bound and free cyt c were quantified by densitometry and normalized by Porin signals. Results are presented in the bar graph as mean ± S.E. (n=3) *, P<0.05 versus free cyt c on pyruvate-malate; **, P<0.05 versus free cyt c on succinate. (B) Same procedure but with brain and liver mitochondria. Second dimensions were probed with anti-cyt c and anti-porin.

loosely-bound free state specifically released by a Ca^{2+}-induced PT.

To illustrate this point, we determined the respiratory rate of mitochondria at state 4 with various energetic substrates and after adding Ca^{2+} (Figure 5C) The uncoupling effect induced by 50 µM Ca^{2+} was observed when the flux increased on succinate, and accentuated on ascorbate-TMPD, but not on pyruvate-malate. However, when the Ca^{2+} concentration increased, the uncoupling effect disappeared even on succinate and respiration was inhibited 2-fold on pyruvate-malate with 100 µM Ca^{2+}. This inhibition was considerably more marked in the presence of CCCP. Moreover, the uncoupling effect on succinate was abolished by adding 10 µM CsA, which specifically inhibits the permeability transition by closing the PTPC. Adding 2mM Ca^{2+}, which was associated with the strong release of cyt *c* from mitochondria observed in Figure 5A, strongly inhibited mitochondrial respiration. These data indicate that the mobilization of cyt *c* by disassociation of the 75 kDa complex may maintain respiration despite a slight release by 50 µM Ca^{2+}. Thus, the mobilized cyt *c* may become involved in electron transfer as well as being releasable by external membrane disruptions. Consequently, functional cyt *c* (electron donor in the respiratory chain) is loosely bound to the mitochondrial inner membrane in free form, unlike the tightly bound form in the 75 kDa complex.

4.5. Respiratory-induced structural changes in ANT1 regulate Bax-triggered cytochrome c release from mitochondria

Previous studies have shown that Bax interacts with ANT to induce a pore-forming structure, leading to the release of cyt *c* and other apoptotic factors from mitochondria (10; 11; 22; 23; 24; 25). By modifying the

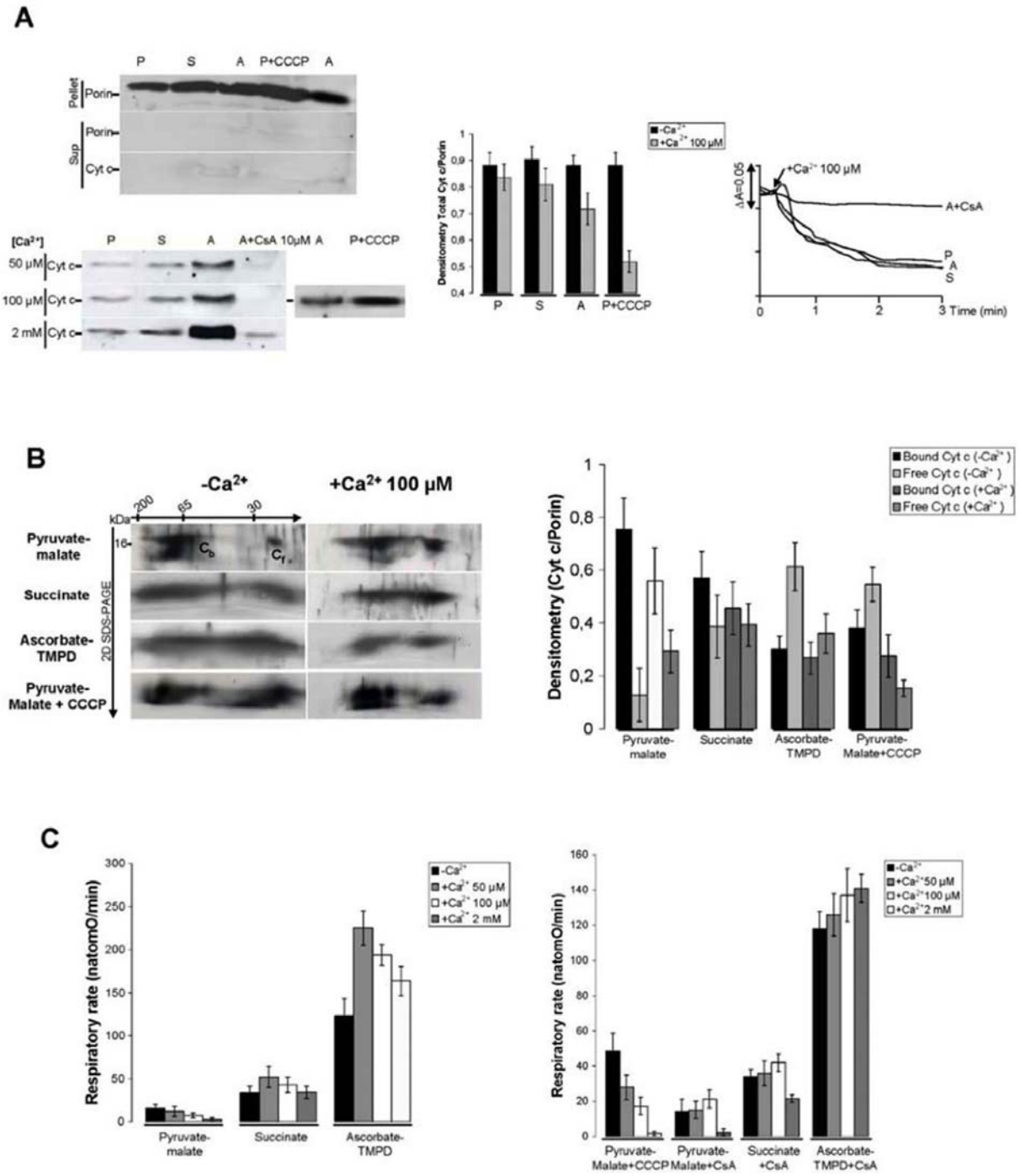

Figure 5. Ca^{2+}-induced PT triggered the release of loosely-bound cyt c involved in respiration. (A) Cyt c release from mitochondria respiring on the various substrates induced by various Ca^{2+} concentrations was quantified by western-blot using anti-cyt c. 100 µM Ca^{2+} was added and mitochondrial swelling (0.5 mg/ml) monitored and measured at 540 nm. (B) Solubilized mitochondria were analyzed on 2D gels and immunoblotted with anti-cyt c. Cyt c was quantified by densitometry and normalized by Porin signals. (C) Respiratory rate of isolated muscle mitochondria (0.5 mg/ml) respiring at state 4 on various substrates, in the presence of various amounts of Ca^{2+}. Results are presented in bar graphs as mean ± S.E. (n=3) *, $P<0.05$ versus pyruvate-malate; **, versus succinate; ❖, versus ascorbate-TMPD. Pyruvate-malate, P; succinate, S; ascorbate-TMPD, A.

experimental procedures (see Material and Methods), on 2D gels of mitochondria respiring on pyruvate-malate and ADP, Bax monomers were associated in distinct complexes exposing the N-ter domain (Figure 6A) Indeed, B_1, B_2,

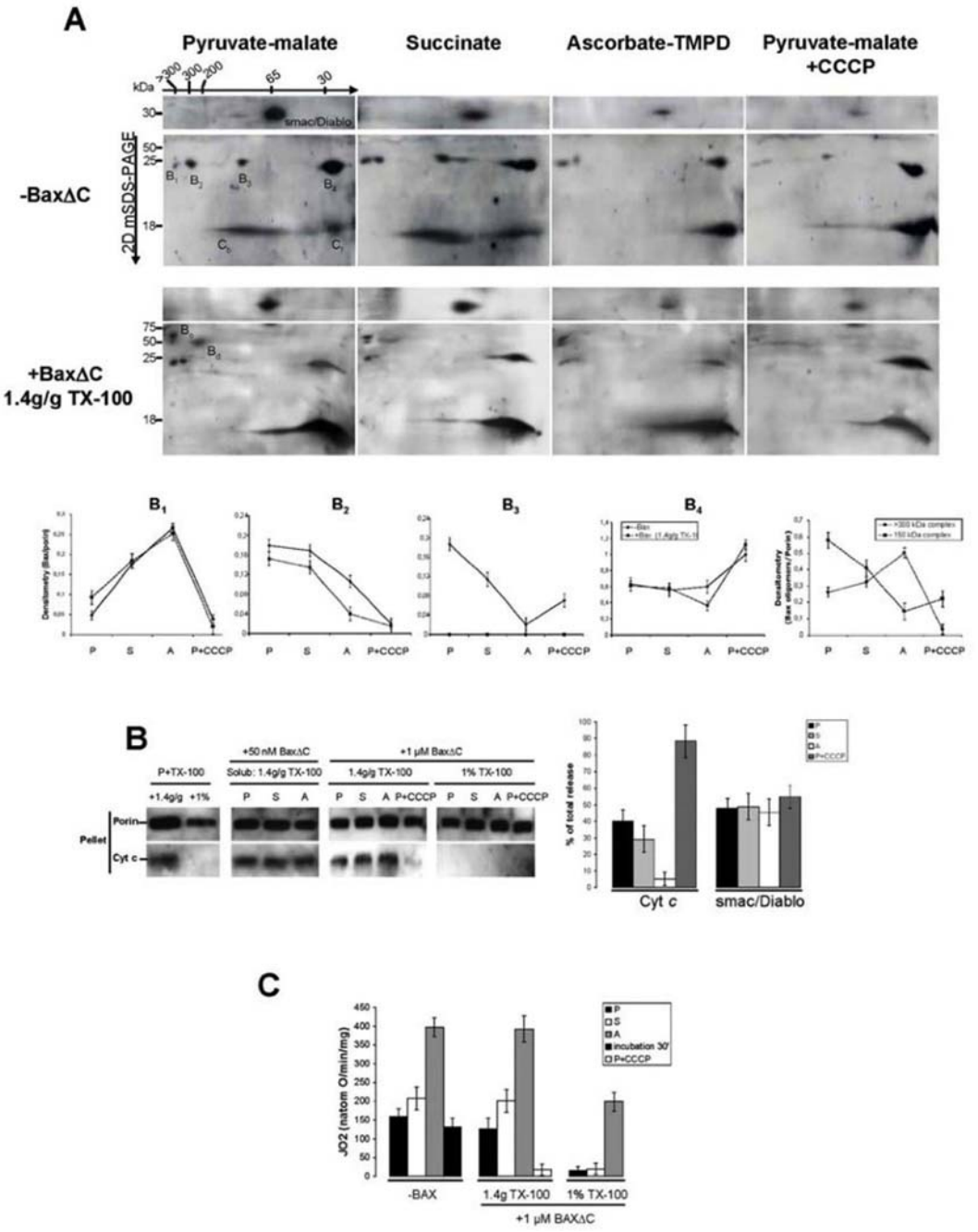

Figure 6. BaxΔC specifically interacts with a structure composed of ANT1 c monomers/cyt c, to form oligomers that release the tightly bound cyt c without affecting mitochondrial functions. (A) 2D gel analysis with 10% BN-PAGE of mitochondria solubilized with digitonin and respiring with ADP on the various substrates, with or without addition of BaxΔC 1 µM previously incubated with TX-100 (1.4 g/g) Second dimensions were immunoblotted with either anti-Bax N-20 and anti-cyt c, or anti-smac/Diablo. Cb, bound cyt c; Cf, free cyt c. Each gel was reprobed with anti-Porin (not shown) to quantify the Bax signals by densitometry (B1; B2; B3; B4; Bd, Bax dimers; Bo, Bax oligomers) Results are presented in curves as mean ± S.E. (n=3) (B) Mitochondria (10 µg) respiring in the presence of the different substrates and incubated with TX-100, or 1 µM BaxΔC/TX-100. After mitochondrial isolation, pellets were subjected to 15% SDS-PAGE and immunoblotted with anti-cyt c and anti-porin. Densitometry analysis (total cyt c in the pellet/porin, and smac/Diablo/porin from the 2D gels above) is shown in the bar graph. (C) Respiratory rate of isolated mitochondria (1 mg/ml) respiring at state 3 on various substrates, in the presence or absence of 1 µM BaxΔC oligomerized with different TX-100 concentrations. Results are presented in the bar graphs as mean ± S.E. (n=3).

and B_3 Bax monomers were observed to interact in complexes exceeding 300 kDa, 300 kDa, and 100 kDa, respectively, whereas B_4 was mainly found in free monomeric form. Several studies have shown that, unlike monomers, the oligomeric form is active in permeabilizing the outer membrane. Thus, inactive endogenous Bax monomers are weakly bound to muscle mitochondria and may interact in specific complexes. Immunoblots with anti-cyt *c* revealed two pools, as previously described. The tightly bound cyt *c* was exactly colocalized with B_3 monomers of Bax associated in a 100 kDa complex. Moreover, 2D gels immunoblotted with anti-smac/Diablo showed 30 kDa monomers in the second dimension associated in 57 kDa dimers from the first dimension. The results obtained on various respiratory substrates show that, like cyt *c*, the Bax monomer in the 100 kDa complex disassociated when respiration increased, resulting in a larger amount of B_1, but not B_4. As in the case of ANT1 oligomerization accompanied by mobilization of bound cyt *c*, this effect is rather marked between succinate and ascorbate-TMPD (B_3 remained undetectable at high respiratory rates) Similarly to ANT1 monomers and cyt *c*, adding CCCP disassociated Bax from the various complexes, increasing B_4. Unlike Bax, SMAC/Diablo was insensitive to respiratory modulations.

To determine the molecular events that occur during the mitochondrial relocation of Bax during apoptosis, we used the same 2D gels as before with purified Bax with the C-terminal domain deleted (BaxΔC) to induce oligomerization of BaxΔC, we previously incubated the protein with various concentrations of TX-100 (Figure 6A) The results of adding BaxΔC (solubilized with TX-100/protein ratio of 1.4 g/g) to isolated mitochondria revealed two new forms i.e. (i) Bax dimers (B_d) maintained in the second dimension (45 kDa), mainly associated in a 150 kDa complex but also in a complex exceeding 300 kDa, and (ii) Bax oligomers (B_o, 65 kDa) in a complex exceeding 300 kDa. B_1 was also observed to increase under these conditions, probably due to disassociation of B_o. However, when BaxΔC was added, B_3 disappeared. When respiration increased, BaxΔC mainly induced modifications in B_3, B_o, and B_d, but not B_1, B_2, and B_4. Indeed, the decrease in B_d in the 150 kDa complex (mainly during the transition from succinate to ascorbate-TMPD) correlated quantitatively with the increase in B_o in a complex exceeding 300 kDa. Thus, respiratory-induced variations in B_d accompanied the oligomerization of ANT1 monomers. Immunoblots with anti-cyt *c* showed that adding BaxΔC induced an increase in C_f by disassociating the cyt *c* bound in the 100 kDa structure. This bound pool was no longer associated with B_d in the 150 kDa complex, irrespective of the substrate used, indicating that B_d was linked to ANT1 *c* monomers and porin, but not cyt *c*.

To investigate whether adding BaxΔC released cyt *c* and whether this effect was sensitive to respiratory changes, we incubated isolated mitochondria respiring with the previous substrates with ADP in the presence of BaxΔC (with 1,4g/g TX-100) Mitochondria were isolated and the pellet immunoblotted with anti-cyt *c* and anti-porin (Figure 6B) The densitometry analysis showed that 50 nM BaxΔC, as well as detergent only, had no effect on the total cyt *c* content of mitochondria respiring on pyruvate-malate, while 1μM BaxΔC released 40% of the total. Contrary to control, this effect was gradually abolished when respiration was increased by succinate and, finally, ascorbate-TMPD (29% and 6%, respectively) Interestingly, adding CCCP strongly enhanced this release (75%) Likewise, adding 1 μM BaxΔC also induced SMAC/Diablo release from mitochondria (48%), but this effect was insensitive to respiratory states. Nevertheless, Figure 6C shows that BaxΔC-induced cyt *c* release at low respiration did not alter the mitochondrial functions. Indeed, despite a strong cyt *c* and smac/Diablo release on pyruvate-malate, the respiratory rate and ATP synthesis (data not shown) remained at control values, emphasizing the absence of $\Delta\psi_m$ and ΔpH collapse, even when 40% of the cyt *c* was released into the cytosol from the mitochondria.

5. DISCUSSION

Previous studies have demonstrated that ANT1 monomers may be mobilized and assembled into active oligomers sensitive to OXPHOS functioning (14). This paper describes six distinct forms of the carrier present in muscle mitochondria under phosphorylation conditions. These forms are distinguished according to their oligomeric (monomers, dimers, or coupled dimers) and conformational states (cytosolic or matricial), as well as associations with other proteins (Figure 7).

These ANT1 structures may feature distinct mitochondrial functions, associated with the respiratory steady-state. M_2 monomers are found in free state, unlike M_1, present in a 95 kDa complex. Moreover, we observed that 80% of the mitochondrial cyt c content interacted in a complex composed of M_1/VDAC1/endogenous Bax monomer, with reinforced binding to the inner membrane. According to the apparent mass restriction, only one or two molecules of cyt *c*, together with a Bax monomer, may interact per complex. These results emphasize the structural specificity of ANT1 c monomers to interact with cyt *c* and endogenous Bax. We show that M_1 and M_2 monomers are able to oligomerize and create new active *c*- and *m*-coupled dimers ($2D_1$, $2D_2$) during a strong increase in respiration, resulting in a metabolic reserve of oxidative phosphorylation (OXPHOS) activity. The tightly bound cardiolipin in the crystallographic structure (26) may be sensitive to $\Delta\psi_m$ or ΔpH changes and induce this assembly.

We evidenced another metabolic reserve mechanism produced by conformational changes in the carrier. 2D gradient gel analysis showed a PTPC-like structure combining ANT1 *c* dimers (D_1) with porin and CyD in a 550-600 kDa complex. These data correlate with those showing that adding CATR or Atr stabilized ANT1 in the *c* conformation required for PTP induction (27), and that ANT1 but not ANT2 is the dominant apoptosis-inducing factor in mammalian cells (28, 29). Four hexokinase isoform 2 (HK 2) molecules and octameric mitochondrial creatine kinase (mtCK) can be added to these structures to form, respectively, the 600 and 400 kDa

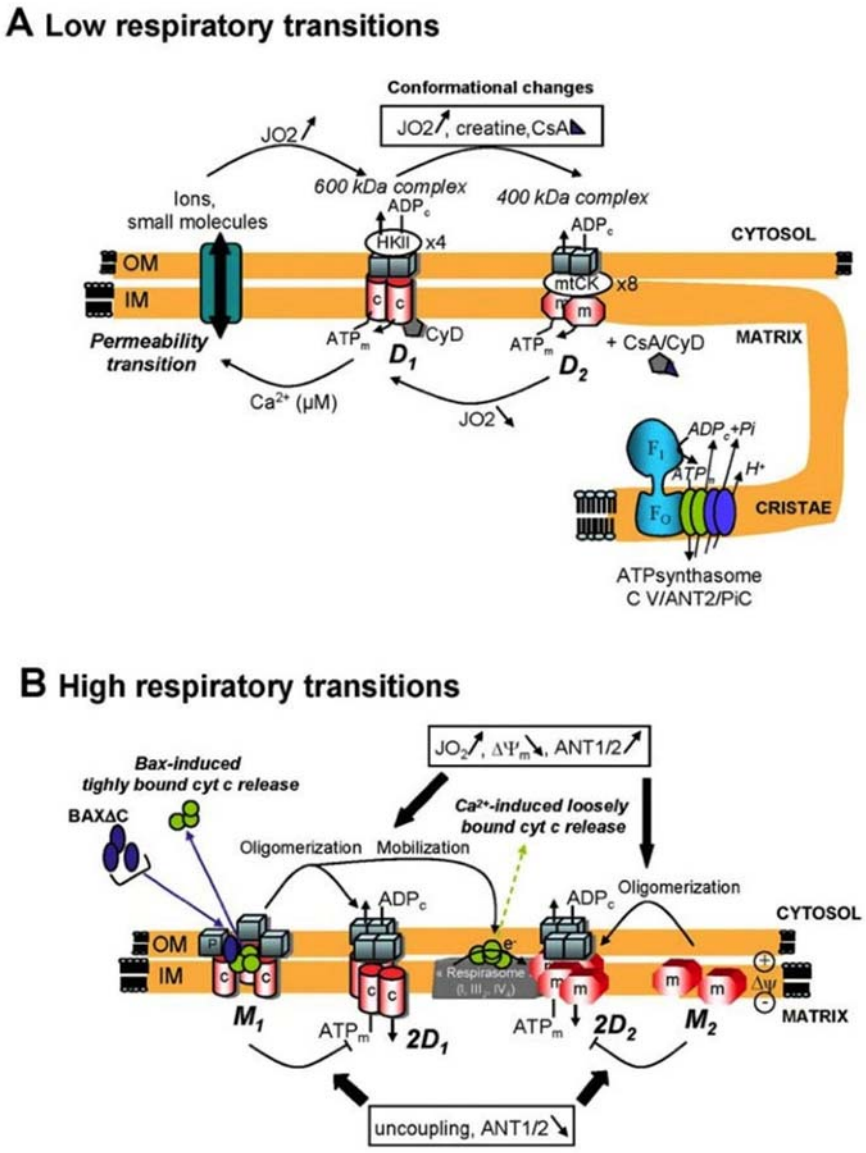

Figure 7. Model of respiratory-dependent regulation of ANT functions between energy supply and apoptosis. This model is based on the identification of direct oligomerization and interactions of ANT1 with other proteins. (A) Conformational modifications at low respiratory transitions of the carrier from the "cytosolic state" (in a PTP-like structure) toward the respiratory active "matricial state" by adding either creatine or CsA. (B) The respiratory-induced mobilization of ANT1 monomers is followed by disassociation of the tightly bound cyt c to the loosely-bound state. Release of the associated cyt c was triggered by BaxΔC, unlike Ca^{2+}-induced PT affecting the free state. HK2, hexokinase isoform 2; mtCK, mitochondrial creatine kinase; c, ANT1 in "cytosolic state"; m, ANT1 in "matricial state"; PCr, phosphocreatine; Cr, creatine; PiC, phosphate carrier; "Respirasome" according to (19).

complexes described by (30). Our experiments demonstrated that an increase in respiration (with succinate or mtCK substrates) induced a conformational change in ANT1 from *c* to *m* (in the 600 and 400 kDa complexes, respectively) (Figure 7) As for the assembly process, the conformational change from *c* to *m* may also result in an increase in ADP/ATP exchange that could be reinforced by channeling with mtCK, as characterized by the 400 kDa complex. Indeed, we observed that the amount of functional ANT in human muscle fibers increased with respiration. Creatine, reported to inhibit the permeability transition (20), induced the same increase as succinate. On the contrary, Ca^{2+}, known to induce a CsA-sensitive permeability transition at low concentrations (He and Lemasters, 2002), reduced the functional ANT involved in nucleotide exchange. Thus, as described for oligomerization (14), this D_1/D_2 transition resulted in the excess of enzyme activity shown in the threshold curves.

This excess maintained a normal respiratory rate until ANT activity had been 80% inhibited. This property can be enhanced by channeling between the mtCK and dimeric ANT *m*. Consequently, this dynamic equilibrium may be regulated by respiratory chain activity. In addition, CsA displaces this equilibrium via the structural effect of closing PTPC (14), whereas creatine induces this transition physiologically via a metabolic effect. These data may explain why different cell energy functioning states (various OXPHOS substrates or other metabolic processes) do not display the same sensitivity towards permeability transition inducers.

Similar mechanisms to ANT involving oligomerization and conformational changes have already been demonstrated for other OXPHOS complexes. Complex I exists in activated and deactivated forms with distinct kinetic and structural properties (30), dimeric Complex III consists of active and "silent" monomers for binding cyt *c* (31), and, finally, dimerization of ATP synthase may be regulated by the matricial pH-dependent binding of the IF1 inhibitor (32) ATP oligomerization is, therefore, involved in the morphology of mitochondrial cristae (33). As for ANT, these molecular mechanisms may be crucial for regulating OXPHOS activity and, thus, the cell energy supply.

Like ANT, cyt *c* displays contrasting functions in mitochondria. Indeed, on the one hand, it is necessary to the cell energy supply as an electron donor within the respiratory chain and, on the other hand, its release activates the apoptosome, thus contributing to the cell death process. It is not yet known how these contrasting pathways are activated according to cell energy status. A recent study shows that cyt *c* may be either loosely or tightly bound to the inner membrane by cardiolipin in liver mitochondria (composed mainly of ANT2). The loosely-bound state is required for cyt *c* release from mitochondria (34). We demonstrated that cyt c was distributed between two distinct pools at low respiratory chain activity, i.e. a large amount associated in a complex composed of ANT1 *c* monomers, a single Bax monomer, and porin, and a minority in free state. Interactions with this complex bind cyt *c* tightly to the inner membrane. These interactions may be hydrophobic or electrostatic between the positively charged Lys of cyt *c* and the negative facing of the external ring of crystallized ANT/CATR complex, rather than the non-polar bonds observed between cyt *c* and the CYT1 subunit of complex III (31). In addition, only the free state of cyt *c* is involved in electron transfer through the respiratory chain, rather than the tightly bound majority stored with the ANT1 *c* monomers. Ca^{2+}-induced PT mobilized the bound cyt *c*, thus increasing the free active pool. At the molecular level, this mechanism is correlated with the CsA-sensitive tBid-induced mitochondrial cristae remodeling required to mobilize cyt *c* stores (35). We observed that only the loosely-bound, active cyt *c* was released under PT with Ca^{2+}, as observed by (13). This probably explains the $\Delta\Psi_m$ collapse observed under these conditions. Indeed, adding Ca^{2+} inhibits respiration for low fluxes and this effect is strongly enhanced with CCCP, which probably disrupts weak interactions between cardiolipin and free monomeric cyt *c*.

On the other hand, we observed that endogenous monomeric inactive Bax associates with ANT1 *c* monomers to constitute an "apoptotic induction unit" (AIU), a specific cyt *c* release pathway capable of inducing a massive release of this component from mitochondria. Indeed, added BaxΔC homodimerized with endogenous monomeric Bax already associated in this structure to mediate a pore-forming structure, releasing large amounts of stored cyt *c* (40% of total). This interaction disassociated the rest of the bound cyt *c*, thus increasing the monomeric respiratory active pool. Therefore, we can postulate that the mitochondrial relocation of the full-length native Bax occurring within cells may form a more efficient structure for releasing the bound cyt *c* completely (without affecting the active pool) These events would make it possible to activate the death pathway while maintaining the respiratory active free cyt *c* in the inner membrane and, thus, the normal rate of respiration and ATP synthesis required for caspase activation. This insight is supported by several studies showing that $\Delta\Psi_m$ collapse is not due to a reduction in the cyt *c* pool, even after a large release into the cytosol (36). Moreover, the effect of Bax on such structure would explain that, once initiated, cyt c is massively and rapidly released from mitochondria without any membrane damage or protein import (37). The time collapse of $\Delta\Psi_m$ downstream from the release step depends on the tissue type and may be due to activated caspases targeting specific sub-units of OXPHOS complexes, such as p75 of Complex I (38). The excess M_1 structure at low fluxes constitutes a fine component for this fast release. Indeed, this structure represents 80% of the cyt c stored with inactive monomers. These mechanisms may impact the cell process as, several cell lines investigated used glucose as a glycolytic rather than a respiratory substrate. Consequently, as Bax-induced cyt *c* release clearly decreased with high respiratory chain activity (unlike Ca^{2+} upload), OXPHOS functioning may regulate the apoptotic induction triggered by Bax. Unlike cyt *c*, dimeric smac/Diablo is free in the intermembrane space and its release is insensitive to respiratory variations. A complex in excess of 300 kDa that is also recognized by exogenous BaxΔC probably mediates its release pathway.

We observed that the oligomerization of ANT1 *c* monomers made it possible for the mobilized cyt *c* to be taken up again in respiration, thus responding to a flux increase while increasing the amount releasable by Ca^{2+}-induced PT. Hence, we may distinguish different cases in terms of the cell's oxidative energy status and sensitivity to different cell-death inducers. Consistent with previous data concerning Bax and Bak regulation of endoplasmic reticulum Ca^{2+} (39), we underline that combined mechanisms, including the permeabilization of OM by "multidomain " Bcl2 family members along with transient PT (triggering tightly- versus loosely-bound cyt *c*) are necessary to fully induce the mitochondrial apoptotic process. Hence, as illustrated in Figure 7, these new insights emphasize the close relationships between structural rearrangements of ANT and molecular apoptotic events at various cell energy levels. OXPHOS functioning has to be, therefore, considered a crucial control point for the events leading to these contrasting pathways.

6. ACKNOWLEDGMENT

This work was supported by INSERM, Université Victor Ségalen-Bordeaux 2, Région Aquitaine, A.F.M. (Association Française contre les Myopathies), F.R.M. (Fondation pour la Recherche Médicale), INCa (Insitut national du Cancer), ANR (Agence Nationale de la Recherche), A.R.C. (Association pour la Recherche contre le Cancer), Philippe Foundation, and the functional genomic facility of the Université Victor Ségalen Bordeaux 2 for mass spectrometry analysis. CB is supported by grants funded by Association pour la Recherche sur le Cancer (ARC), EGIDE, l'Agence Nationale pour la Recherche (ANR, ANR-08PCVI-0008-01) and l'Institut National pour le Cancer (INCa, 2008-1-PL BIO-04-CNRS ON1). The authors thank O. Sharaf el dein for his help in preparation of the manuscript.

7. REFERENCES

1. Klingenberg, M. Structure-function of the ADP/ATP carrier. *Biochem Soc Trans*, 20, 547-550 (1992)

2. Boulay, F., Lauquin, G.J. & Vignais, P.V. Localization of immunoreactive regions in the beef heart adenine nucleotide carrier using rabbit antisera against the carboxyatractyloside-liganded and the sodium dodecyl sulfate denaturated carrier forms. *Biochemistry*, 25, 7567-7571 (1986)

3. Levy, S.E., Chen, Y.S., Graham, B.H. & Wallace, D.C. Expression and sequence analysis of the mouse adenine nucleotide translocase 1 and 2 genes. *Gene*, 254, 57-66 (2000)

4. Huang, S.G., Odoy, S. & Klingenberg, M. Chimers of two fused ADP/ATP carrier monomers indicate a single channel for ADP/ATP transport. *Arch Biochem Biophys*, 394, 67-75 (2001)

5. Block, M.R. & Vignais, P.V. Substrate-site interactions in the membrane-bound adenine-nucleotide carrier as disclosed by ADP and ATP analogs. *Biochim Biophys Acta,* 767, 369-376 (1984)

6. Kaukonen, J., Juselius, J.K., Tiranti, V., Kyttala, A., Zeviani, M., Comi, G.P., Keranen, S., Peltonen, L. & Suomalainen, A. Role of adenine nucleotide translocator 1 in mtDNA maintenance. *Science*, 289, 782-785 (2000)

7. Halestrap, A. Biochemistry: a pore way to die. *Nature*, 434, 578-579 (2005)

8. Kroemer G, Galluzzi L, & Brenner C. Mitochondrial membrane permeabilization in cell death. *Physiol Rev*. 2007;87:99-163 (2007)

9. Zamzami, N. & Kroemer, G. The mitochondrion in apoptosis: how Pandora's box opens. *Nat Rev Mol Cell Biol*, 2, 67-71 (2001)

10. Marzo, I., Brenner, C., Zamzami, N., Jurgensmeier, J.M., Susin, S.A., Vieira, H.L., Prevost, M.C., Xie, Z., Matsuyama, S., Reed, J.C. & Kroemer, G. Bax and adenine nucleotide translocator cooperate in the mitochondrial control of apoptosis. *Science*, 281, 2027-2031 (1998)

11. Pastorino JG, Tafani M, Rothman RJ, Marcinkeviciute A, Hoek JB, & Farber JL. Functional consequences of the sustained or transient activation by Bax of the mitochondrial permeability transition pore. *J Biol Chem.* 274:31734-9 (1999)

12. Eskes R, Antonsson B, Osen-Sand A, Montessuit S, Richter C, Sadoul R, Mazzei G, Nichols A, & Martinou JC. Bax-induced cytochrome C release from mitochondria is independent of the permeability transition pore but highly dependent on Mg2+ ions. *J Cell Biol.* 143:217-24 (1998)

13. von Ahsen, O., Renken, C., Perkins, G., Kluck, R.M., Bossy-Wetzel, E. & Newmeyer, D.D. Preservation of mitochondrial structure and function after Bid- or Bax-mediated cytochrome c release. *J Cell Biol*, 150, 1027-1036 (2000)

14. Faustin, B., Rossignol, R., Rocher, C., Benard, G., Malgat, M. & Letellier, T. Mobilization of adenine nucleotide translocators as molecular bases of the biochemical threshold effect observed in mitochondrial diseases. *J Biol Chem*, 279, 20411-20421 (2004)

15. Rossignol, R., Malgat, M., Mazat, J.-P. & Letellier, T. Threshold Effect and Tissue Specificity. *J Biol Chem* 274, 33426-33432 (1999)

16. Letellier, T., Malgat, M., Coquet, M., Moretto, B., Parrot-Roulaud, F. & Mazat, J.P. Mitochondrial myopathy studies on permeabilized muscle fibers. *Pediatr Res*, 32, 17-22 (1992).

17. Chance, B. & Williams, G.R. *Adv. Enzymol.*, 17, 65-134 (1956)

18. Jurgensmeier, J.M., Xie, Z., Deveraux, Q., Ellerby, L., Bredesen, D. and Reed, J.C. Bax directly induces release of cytochrome c from isolated mitochondria. *Proc Natl Acad Sci U S A*, 95, 4997-5002 (1998)

19. Schägger, H. & Pfeiffer, K. Supercomplexes in the respiratory chains of yeast and mammalian mitochondria. *EMBO J*, 19, 1777-1783 (2000)

20. Dolder, M., Walzel, B., Speer, O., Schlattner, U. & Wallimann, T. Inhibition of the mitochondrial permeability transition by creatine kinase substrates. Requirement for microcompartmentation. *J Biol Chem*, 278, 17760-17766 (2003)

21. Kroemer, G. & Reed, J.C. Mitochondrial control of cell death. *Nat Med*, 6, 513-519 (2000)

22. Brenner C, Cadiou H, Vieira HL, Zamzami N, Marzo I, Xie Z, Leber B, Andrews D, Duclohier H, Reed JC & Kroemer G. Bcl-2 and Bax regulate the channel activity of the mitochondrial adenine nucleotide translocator. *Oncogene.* 19:329-36 (2000)

23. Cao G, Minami M, Pei W, Yan C, Chen D, O'Horo C, Graham SH, & Chen J. Intracellular Bax translocation after transient cerebral ischemia: implications for a role of the mitochondrial apoptotic signaling pathway in ischemic neuronal death. *J Cereb Blood Flow Metab.* 2, 321-33 (2001)

24. Capano M & Crompton M. Biphasic translocation of Bax to mitochondria. *Biochem J.* 367:169-78 (2002).

25. Belzacq AS, Vieira HL, Verrier F, Vandecasteele G, Cohen I, Prévost MC, Larquet E, Pariselli F, Petit PX, Kahn A, Rizzuto R, Brenner C & Kroemer G. Bcl-2 and Bax modulate adenine nucleotide translocase activity. *Cancer Res.* 63:541-6 (2003)

26. Pebay-Peyroula, E., Dahout-Gonzalez, C., Kahn, R., Trezeguet, V., Lauquin, G.J. & Brandolin, G. Structure of mitochondrial ADP/ATP carrier in complex with carboxyatractyloside. *Nature*, 426, 39-44 (2003)

27. Davidson, A.M. &Halestrap, A.P. Liver mitochondrial pyrophosphate concentration is increased by Ca2+ and regulates the intramitochondrial volume and adenine nucleotide content. *Biochem J*, 246, 715-723 (1987)

28. Bauer, M.K., Schubert, A., Rocks, O. & Grimm, S. Adenine nucleotide translocase-1, a component of the permeability transition pore, can dominantly induce apoptosis. *J Cell Biol,* 147, 1493-1502 (1999)

29. Le Bras M, Borgne-Sanchez A, Touat Z, El Dein OS, Deniaud A, Maillier E, Lecellier G, Rebouillat D, Lemaire C, Kroemer G, Jacotot E, & Brenner C. Chemosensitization by knockdown of adenine nucleotide translocase-2. Cancer Res. 66:9143-52 (2006)

30. Beutner, G., Ruck, A., Riede, B. & Brdiczka, D. Complexes between porin, hexokinase, mitochondrial creatine kinase and adenylate translocator display properties of the permeability transition pore. Implication for regulation of permeability transition by the kinases. *Biochim Biophys Acta,* 1368, 7-18 (1998)

31. Lange, C. & Hunte, C. Crystal structure of the yeast cytochrome bc1 complex with its bound substrate cytochrome c. *Proc Natl Acad Sci U S A*, 99, 2800-2805 (2002)

32. Cabezon, E., Montgomery, M.G., Leslie, A.G. &Walker, J.E. The structure of bovine F1-ATPase in complex with its regulatory protein IF1. *Nat Struct Biol*, 10, 744-750 (2003)

33. Paumard, P., Vaillier, J., Coulary, B., Schaeffer, J., Soubannier, V., Mueller, D.M., Brethes, D., di Rago, J.P. & Velours, J. (2002) The ATP synthase is involved in generating mitochondrial cristae morphology. *Embo J*, 21, 221-230.

34. Ott, M., Robertson, J.D., Gogvadze, V., Zhivotovsky, B. & Orrenius, S. Cytochrome c release from mitochondria proceeds by a two-step process. *Proc Natl Acad Sci U S A*, 99, 1259-1263 (2002)

35. Scorrano, L., Ashiya, M., Buttle, K., Weiler, S., Oakes, S.A., Mannella, C.A. & Korsmeyer, S.J. A distinct pathway remodels mitochondrial cristae and mobilizes cytochrome c during apoptosis. *Dev Cell*, 2, 55-67 (2002)

36. Waterhouse, N.J., Goldstein, J.C., von Ahsen, O., Schuler, M., Newmeyer, D.D. & Green, D.R. Cytochrome c maintains mitochondrial transmembrane potential and ATP generation after outer mitochondrial membrane permeabilization during the apoptotic process. *J Cell Biol*, 153, 319-328 (2001)

37. Goldstein, J.C., Waterhouse, N.J., Juin, P., Evan, G.I. & Green, D.R. The coordinate release of cytochrome c during apoptosis is rapid, complete and kinetically invariant. *Nat Cell Biol*, 2, 156-162 (2000)

38. Ricci, J.E., Munoz-Pinedo, C., Fitzgerald, P., Bailly-Maitre, B., Perkins, G.A., Yadava, N., Scheffler, I.E., Ellisman, M.H. & Green, D.R. Disruption of mitochondrial function during apoptosis is mediated by caspase cleavage of the p75 subunit of complex I of the electron transport chain. *Cell*, 117, 773-786 (2004)

39. Scorrano, L., Oakes, S.A., Opferman, J.T., Cheng, E.H., Sorcinelli, M.D., Pozzan, T. & Korsmeyer, S.J. BAX and BAK regulation of endoplasmic reticulum Ca2+: a control point for apoptosis. *Science*, 300, 135-139 (2003)

Abbreviations: Abs, antibodies; ADP, adenosine diphosphate; ATP, adenosine triphosphate; ANT, adenine nucleotide translocator; BN-PAGE, blue-native polyacrylamide gel electrophoresis; CATR, carboxyatractyloside; cyt *c*, cytochrome *c*; CsA, cyclosporin A; CyD, cyclophiline D; JO_2, respiratory rate; SDS-PAGE, sodium dodecyl sulfate-polyacrylamide gel electrophoresis; PTPC, permeability transition pore complex; TMPD, *N,N,N',N'*-tetramethyl-*p*-phenylenediamine; OXPHOS, oxidative phosphorylation

Key Words: Apoptosis, Bax, Mitochondria, Metabolism, Respiration

Send correspondence to: Thierry Letellier, 1INSERM U688, Universite Victor Segalen-Bordeaux 2, 146 rue Leo-Saignat, F-33076 Bordeaux Cedex, France, Tel: 33-557571657, Fax: 33-557571431, E-mail: thierry.letellier@u-bordeaux2.fr

http://www.bioscience.org/current/vol3E.htm